sustainability

MDPI

Article

Analysis of Environmental Impact and Mechanical Properties of Inconel 625 Produced Using Wire Arc Additive Manufacturing

J. Iain Sword, Alexander Galloway and Athanasios Toumpis *

Department of Mechanical & Aerospace Engineering, University of Strathclyde, James Weir Building, 75 Montrose Street, Glasgow G1 1XJ, UK
* Correspondence: athanasios.toumpis@strath.ac.uk

Abstract: Inconel 625 is a nickel-based superalloy widely used in industries such as energy, space, and defence, due to its strength and corrosion resistance. It is traditionally time- and resource-intensive to machine, leading to increased environmental impact and material waste. Using additive manufacturing (AM) technology enables a reduction in resource consumption during the manufacture of high value components, as material is only deposited where it is required. This study compares the environmental impact of manufacturing an Inconel 625 impeller through machining and wire arc additive manufacturing (WAAM) by employing established life cycle assessment methods. WAAM shows significant advantages, cutting energy consumption threefold and reducing material waste from 85% to 35%. The current work also evaluates the mechanical properties of WAAM-produced components through tensile and axial fatigue testing, in addition to the use of optical and electron microscopy for metallurgical analysis and fractography. This demonstrates yield and ultimate tensile strengths exceeding industrial standards, with comparable or superior fatigue life to other AM methods. The improved fatigue performance extends the service life of components, bolstering sustainability by reducing the need for frequent replacements, thereby lessening associated environmental impacts. These findings underscore the promise of WAAM in enhancing both environmental sustainability and mechanical performance in manufacturing Inconel 625 components.

Keywords: wire arc additive manufacturing; metal additive manufacturing; Inconel 625; sustainable manufacturing; mechanical testing

Citation: Sword, J.I.; Galloway, A.; Toumpis, A. Analysis of Environmental Impact and Mechanical Properties of Inconel 625 Produced Using Wire Arc Additive Manufacturing. *Sustainability* **2024**, *16*, 4178. https://doi.org/10.3390/su16104178

Academic Editors: Jinoop Arackal Narayanan, Farzaneh Kaji, Sunil Pathak and Ehsan Toyserkani

Received: 19 April 2024
Revised: 10 May 2024
Accepted: 14 May 2024
Published: 16 May 2024

1. Introduction

Inconel 625 is a nickel alloy widely used in industries such as energy, space, and defence due to its strength at high temperatures and corrosion resistance [1]. This alloy undergoes solid-solution strengthening by introducing chromium and molybdenum, as well as the formation of carbides of niobium and chromium [2]. Niobium is also noted to form the metastable strengthening phase γ″, which stabilises to form the δ phase with a high temperature service [3]. This results in alloys well suited for extreme service conditions such as gas turbines [4], corrosive environments [5], and space propulsion systems [6,7].

Components manufactured from Inconel 625, such as turbine impellers or valve parts, often have complex geometries due to the demands on their design. These components are typically machined from a solid billet of material [8], leading to a high proportion of material wasted. The production and machining of this alloy is costly and has a high environmental impact compared to other engineering materials [9]. As such, novel technologies to reduce the material waste and environmental impact of production are being investigated by the manufacturing sector [10].

One method of reducing the environmental impact of manufacturing complex components is to adopt additive manufacturing (AM) [11]. In contrast to subtractive manufacturing techniques such as milling and turning, AM techniques build up a component incrementally from a feedstock such as a powder or wire [12]. This family of processes is

applicable to a range of materials including metals [13], polymers [14] and ceramics [15]. In this field, wire arc additive manufacturing (WAAM) is promising [16,17]. This process is capable of depositing components with mechanical properties comparable to equivalent wrought alloys [18] at a high deposition rate [19]. However, the dimensional precision of this method is low due to a large melt pool during deposition [20].

The properties of WAAM-deposited Inconel 625 have been the subject of recent research efforts. These extend to the microstructure and mechanical properties when manufactured using different variants of the WAAM process. These variants include cold metal transfer (CMT) [21] and gas tungsten arc welding (GTAW) [22]. Moreover, changes in different parameters such as travel speed [23] and post-weld heat treatment (PWHT) [24,25] have been investigated. An additional factor which is important for engineering components is their response to cyclic loading which has been identified as a challenge for rotating systems since 1858 [26]. The fatigue performance of Inconel 625 has previously been assessed for material produced through a range of processes, including powder metallurgy (PM-HIP) [27], laser powder bed fusion (LPBF) [28], and welded plates [29]. The results presented in this study for WAAM-produced material will be compared with the previously published literature to determine its suitability for use in industry as a replacement for existing processes.

A life cycle assessment (LCA) can be performed on engineering components to analyse and compare the environmental impact of manufacturing processes. This quantifies the effect of every input and output during manufacture, operation and decommissioning [30]. An LCA considers a range of factors which impact the environment. Examples include the production of chemical waste products, the utilisation of raw materials, and the consumption of energy [31]. Many high level LCAs will consider the embodied energy and CO_2 emissions [32]. When more detail is required, other metrics such as the acidification and toxification potential can be considered [33–35].

Previous LCAs of engineered products have shown that a significant contributor to the environmental impact is the extraction and primary production of materials [34,36]. In addition, the environmental impact of WAAM has been previously studied, in comparison with other common manufacturing techniques such as forging, casting and machining for a range of materials [11,32,37].

This novel investigation expands on previous literature by presenting the environmental benefit alongside the mechanical properties of an additively manufactured Inconel 625 impeller. The results of this study demonstrate strong advantages for the adoption of WAAM for industrial manufacturing when compared to conventional manufacturing. The LCA determines the difference in environmental impact metrics such as energy consumption, CO_2 emissions and material waste between WAAM production and conventional machining. The analysis of the microstructure and mechanical properties considers the dominant phases, hardness, tensile strength and fatigue performance of the alloy. The results are compared against existing literature [25] and relevant standards [38].

2. Materials and Methods

2.1. Life Cycle Analysis

The method for conducting an LCA of components produced through WAAM has been described previously [11]. This process is compared against machining, the conventional manufacturing process for an Inconel 625 impeller. Forging has been demonstrated to be a possible alternative, but has not been widely adopted for the manufacture of impellers due to its complexity; therefore, it has not been included in this analysis [8]. The material flows for the WAAM process are shown in Figure 1.

The impeller was generated using 3D modelling software (Solidworks 2023), with an approximation of the manufacturing processes applied to the model to determine the mass added or removed at each stage. These models are shown in Figure 2.

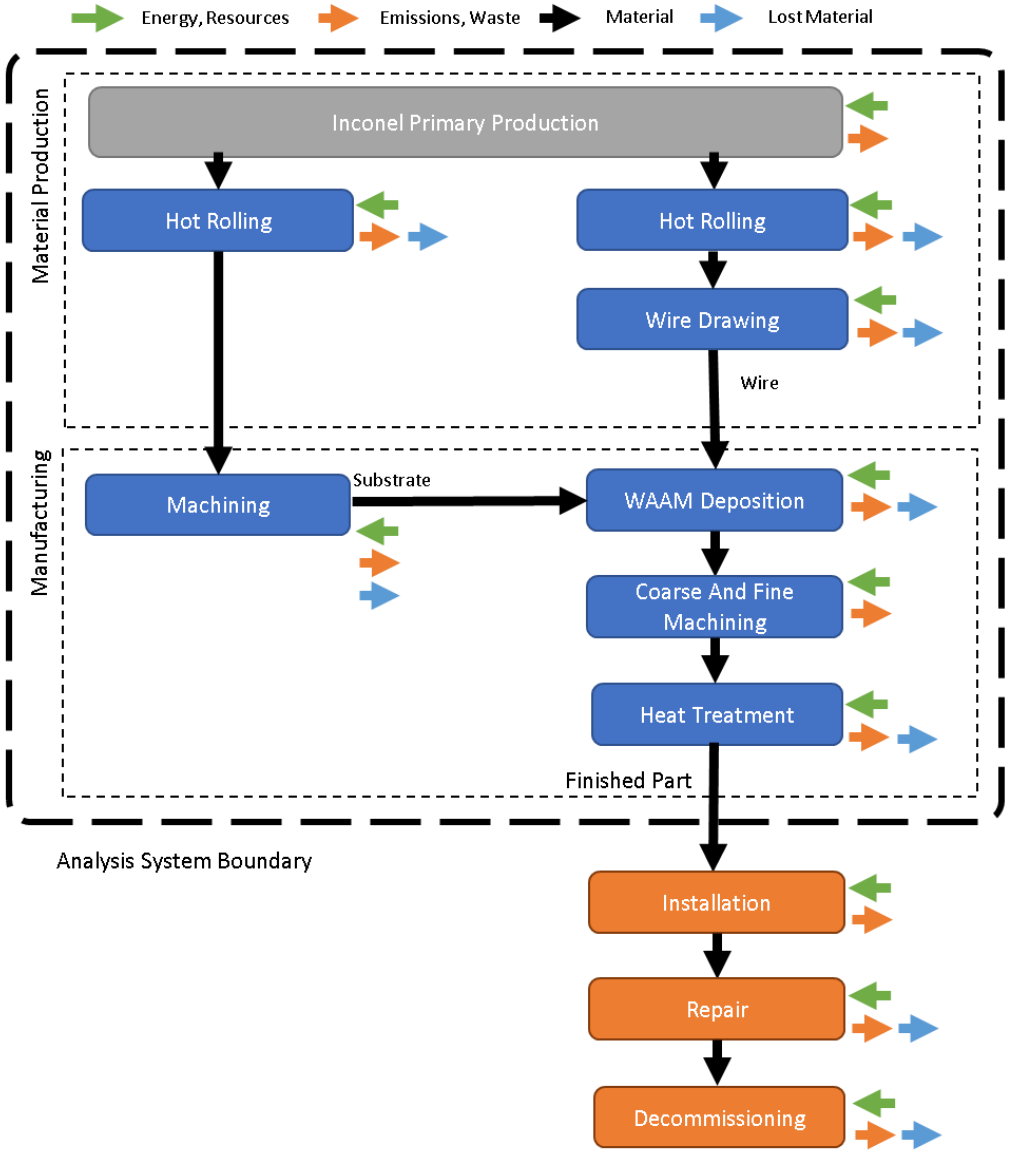

Figure 1. Resource flow diagram for the WAAM process (adapted from Sword et al. [11]). Blue processes indicate industrial manufacturing processes, grey indicates primary production, while orange represents actions taken by an end-user.

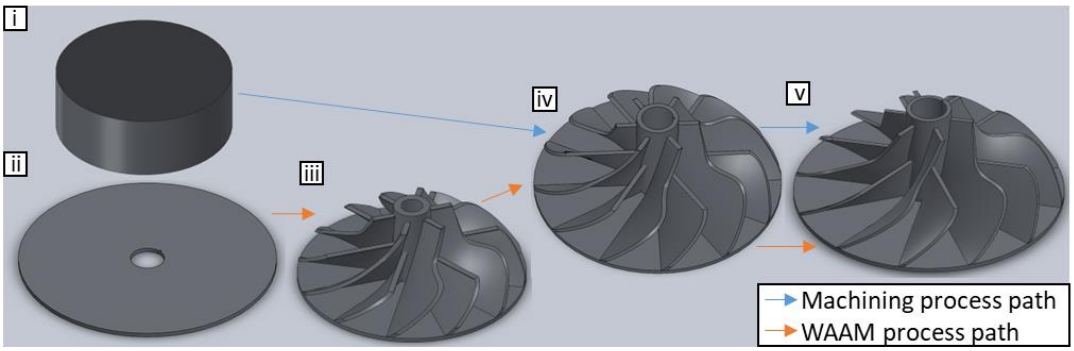

Figure 2. Manufacturing stages for life cycle assessment. (**i**) Rolled billet for machining, (**ii**) substrate for deposition, (**iii**) result of WAAM deposition, (**iv**) result of coarse machining, and (**v**) result of fine machining (finished component).

The energy consumption and carbon emissions of the WAAM process are adapted from a general assessment of the energy required for WAAM by Priarone et al. [32]. Carbon emissions are determined using the carbon emission signature (*CES*) [39], which will be calculated for the global average supply of energy [40]. Data gathered from literature was used for machining and primary production of materials [9]. The energy consumption required for heat treatment is determined using data previously obtained for a top-hat furnace employed in industrial heat treatment and used in a previous study [11].

2.2. Material Testing

The bulk material produced for this work was a wall of deposited material with the following dimensions: 235 mm × 30 mm × 110 mm. This was manufactured using an AM cell. This cell was composed of an ABB 2400 L robot arm (ABB, Tokyo, Japan) controlled by an ABB IRC5 control cabinet (ABB, Tokyo, Japan) and teach pendant in addition to a Fronius cold metal transfer (CMT) fusion welding torch (Fronius, Wels, Austria), power supply and wire feed.

The shielding gas was 70% argon and 30% helium at 22 L/min and the substrate was EN32B low carbon mild steel. Commercially available ERNiCrMo-3 welding wire of 1.2 mm diameter (WL allotech, Changzhou, China) was used as a feedstock; the chemical composition of the feedstocks is shown in Table 1 as provided in the suppliers' datasheets.

Table 1. Chemical composition of material feedstocks.

Chemical Element %	Material	Ni	Cr	Fe	Nb	Mo	Ti
Filler Wire	ERNiCrMo-3	64	22.5	0.2	3.9	9.5	0.22
Substrate	EN32B	-	-	Bal.	-	-	-
Chemical Element %	**Material**	**Cu**	**Mn**	**Si**	**C**	**P**	**S**
Filler Wire	ERNiCrMo-3	0.1	0.05	0.05	0.1	0.01	0.001
Substrate	EN32B	-	0.70	0.22	0.15	0.016	0.010

The process parameters are shown in Table 2, as these were obtained from settings within the robot and weld control systems with interpass temperature measured using a digital thermometer probe. Heat input was calculated using Equation (1) from BE EN 1011-1. In this equation, Q is the heat input and k is the thermal efficiency (0.8 for MIG welding) [41]. V and I are the voltage and current of the arc and v is the arc travel speed.

Table 2. Process parameters for WAAM production.

Travel Speed (mm/s)	Wire Feed Speed (m/min)	Standoff Distance (mm)	Interpass Temperature (°C)	Travel Speed (mm/s)	Wire Feed Speed (m/min)	Standoff Distance (mm)	Interpass Temperature (°C)
13	6.5	8	60	13	6.5	8	60
Current (A)	**Voltage (V)**	**Weave**	**Energy Input (kJ/mm)**	**Current (A)**	**Voltage (V)**	**Weave**	**Energy Input (kJ/mm)**
178	17.4	none	0.191	178	17.4	none	0.191

Heat treatment was performed using a Carbolite RHF1500 furnace (Carbolite, Hope Valley, UK) after wrapping in stainless steel foil to reduce the formation of oxide scale on the material. Details of the heat treatments and associated mechanical properties are given in Table 3 as presented in the standard ASTM B443 [38].

$$Q = k\frac{V \cdot I}{v} \cdot 10^{-3} \text{ in kJ/mm} \quad (1)$$

Table 3. Heat treatment parameters and mechanical properties for Inconel 625 [37].

Heat Treatment	Temperature (°C)	Time (h)	Yield Strength (MPa)	Tensile Strength (MPa)	Elongation (%)	Hardness (HV)
Solution Treated	1150	2	276	690	30	124–197

Samples were extracted from the bulk wall and prepared by standard metallographic grinding and polishing techniques followed by electro-etching with oxalic acid. Examination of the microstructure was performed using an Olympus GX51 inverted microscope (Olympus, Tokyo, Japan). Microhardness measurements were taken on these same samples using a Q-Ness 60A+ automated hardness tester (ATM Qness GmbH, Mammelzen, Germany) with a 0.05 kg load.

Tensile and fatigue samples were produced from the bulk material as indicated in Figure 3. The tensile and fatigue testing samples were extracted from the bulk material by water jet cutting before milling to shape. The dimensions of these samples were derived from standards ASTM-E8 [42] and BS EN ISO 148 [43], respectively. Tensile and fatigue testing was performed using an Instron 8802 servo-hydraulic universal testing machine with a capacity of 250 kN in accordance with ASTM-E8 and ASTM-E466 [44].

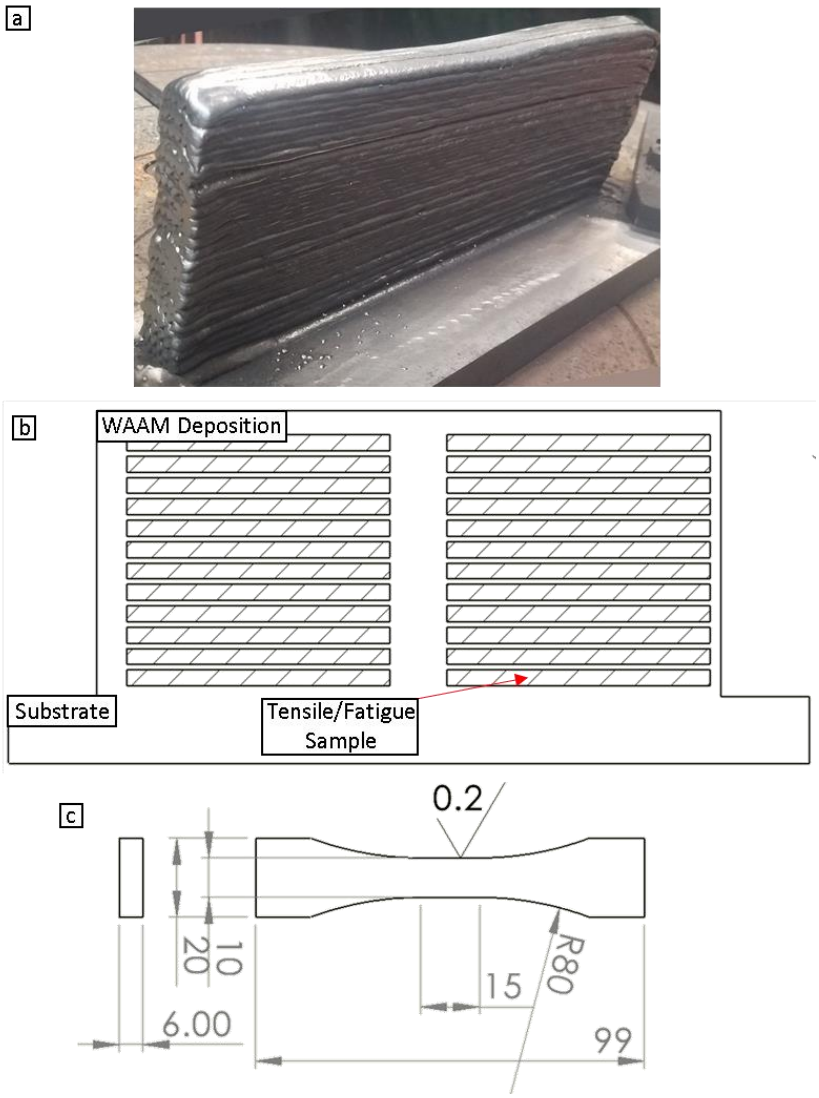

Figure 3. (**a**) Image of the deposited wall of material; (**b**) schematic of individual samples extracted from deposited material; (**c**) dimensions of tensile and fatigue samples.

All fatigue tests were performed on the Instron 8802 with a loading ratio of 0.1 and cycle frequency of 10 Hz, using the same sample design as for tensile testing. This incorporated a surface finish of Ra < 0.2 µm and a large radius of transition between the grips and reduced area. For this testing regime, 15 samples were tested at 4 stress ranges given as a percentage of yield stress from 100 to 160%.

3. Results and Discussion

3.1. Life Cycle Analysis

The first stage of this LCA is to determine the mass of the component at each stage of production. When combined with process data, this allows the CO_2 emissions and energy consumption for each stage to be determined. Combining these contributions gives the total environmental impact for the process which can then be compared directly with other processes. The mass breakdown for this component, gathered from CAD software, is shown in Table 4. The process parameters used for WAAM deposition are presented in Table 5, allowing for the calculation of environmental impact metrics.

Table 4. Mass breakdown for component production by WAAM.

Component Mass Breakdown (kg)		
Process	**WAAM**	**Machining**
Rolled Billet (Substrate)	3.84	73.605
Deposition	6.763	-
Coarse Machining	−2.969	−65.971
Fine Machining	−0.805	−0.805
Component Total	6.805	6.805
Rolled Billet (Substrate)	3.84	73.605

Table 5. Process parameters for WAAM used in environmental analysis.

WAAM Process Parameter	
Deposition Rate (ideal)	3.74 kg/h
Arc Power	3.0972 kW
Standby Power	0.1 kW
Start-up Time	1
Arc Time	1.85 h
Gas Flow Time	1.85 h
Build Time	1.85 h
Gas Flow Rate	1320 L/h

Using the data collected for both WAAM and machining, the primary energy and CO_2 emissions for the production of an Inconel 625 impeller are tabulated in Tables 6 and 7; the results are then presented in Figures 4 and 5, where the error bars are defined as the difference between the maximum and minimum values for each contribution. These results show that for the machined component, the greatest contribution to energy consumption is the primary production of Inconel 625. Due to the reduction in required material, the contribution of primary production to the WAAM component is dramatically reduced.

Table 6. Energy consumption and CO_2 emissions for the component produced by WAAM.

Process	Primary Energy (MJ)	Carbon Dioxide ($kgCO_2eq$)
WAAM Idle	1.059	1.936
WAAM Deposition	60.51	110.63
WAAM Shielding Gas	2.987	5.461
WAAM Total	64.56	118.03
Wire Primary Production	1560.5	103.93
Substrate Primary Production	818.5	54.52

Table 6. *Cont.*

Process	Primary Energy (MJ)	Carbon Dioxide ($kgCO_2eq$)
Wire Drawing	168.7	12.62
Substrate Rolling	13.82	1.038
Coarse Machining	8.262	0.2188
Fine Machining	4.287	0.322
Heat Treatment	2645.2	4836.1
Total	5283.8	5126.8

Table 7. Energy consumption and CO_2 for the component produced by machining.

Process	Primary Energy (MJ)	Carbon Dioxide ($kgCO_2eq$)
Billet Primary Production	15,336	1021.4
Billet Rolling	258.7	19.43
Coarse Milling	64.78	4.862
Fine Milling	4.287	0.322
Heat Treatment	2645.2	4836.1
Total	18,244	5877.3

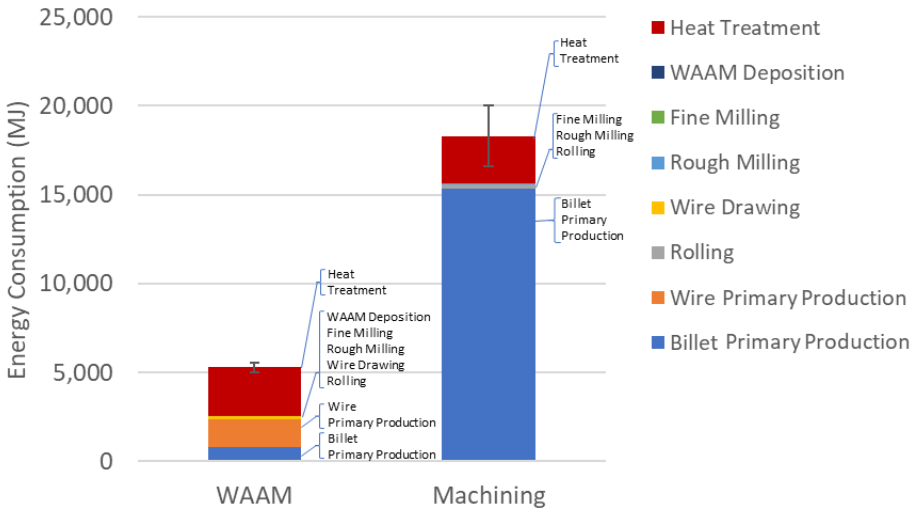

Figure 4. Energy consumption required to produce the component.

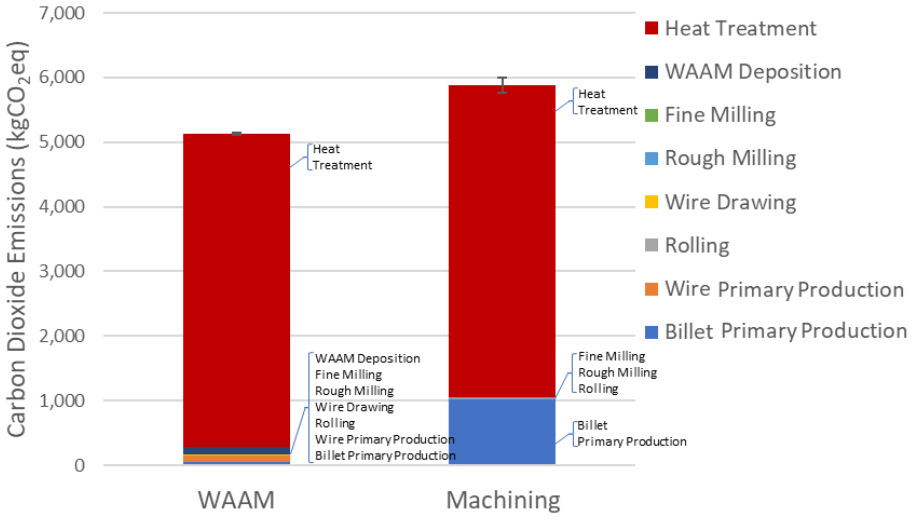

Figure 5. CO_2 emissions produced during manufacture of the component.

This causes the heat treatment process to be responsible for the greatest proportion of the total energy consumption during WAAM. When the CO_2 emissions are compared, the gap is reduced, with emissions being dominated by the equal contribution of heat treatment between both processes. As discussed in Section 3.2, this heat treatment is required for this material to dissolve detrimental phases such as the Laves phase. The dominance of this process is caused by the significant energy requirements and the conversion factor being based on global averages for carbon emissions for energy production [39,40]. This conversion factor is greater than those used elsewhere [9], so aspects of production calculated using the CES conversion are more heavily weighted.

The results are compared in Table 8 using the material waste percentage, specific energy consumption and specific CO_2 emissions. In Figure 6, these metrics are normalised against the results determined for WAAM to provide a direct comparison between the processes. These results show the dramatic difference between the material wasted during WAAM and machining, and the difference in energy consumption required by both processes. A total material waste figure has also been included, accounting for losses during rolling and wire drawing. The specific metrics can also be compared to previous data from an LCA of a WAAM-produced titanium component [11]. In this case, the specific energy consumption and CO_2 emissions were found to be higher than those reported in the previous study. These increases can be explained by the higher arc energy and heat treatment temperature, in addition to the reduced mass of the Inconel component, leading to a decrease in economies of scale for aspects of production which do not scale with mass such as heat treatment.

Table 8. Environmental impact metrics and specific impact by process.

	WAAM	Machining
Manufacturing Material Waste (%)	35.82	86.43
Total Material Waste (%)	42.80	91.20
Energy Consumption (MJ)	5283.8	18244
Specific Energy Consumption (MJ/kg)	776.45	2681.0
Carbon Emissions ($kgCO_2eq$)	5126.8	5877.3
Specific Carbon Emissions ($kgCO_2eq/kg$)	753.4	863.7

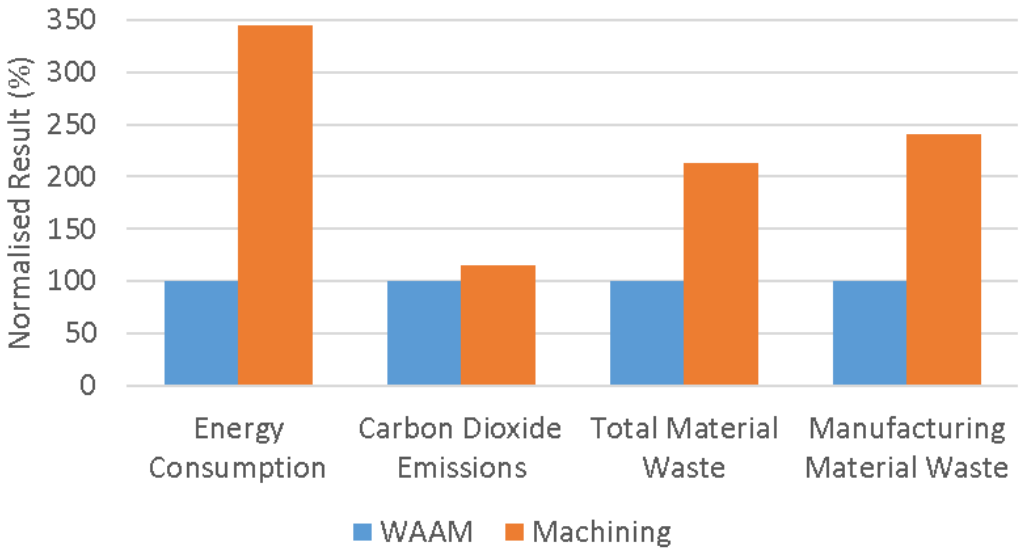

Figure 6. Normalised comparison of environmental metrics.

The results of this LCA demonstrate a significant reduction in the environmental impact through the adoption of WAAM to replace machining for the manufacture of an Inconel 625 impeller. The most dramatic reductions are of the energy consumption and

material waste, while a small reduction in CO_2 emissions is noted (Figure 6). This reduction in environmental impact is caused by a decrease in the material required for the component when compared to machining from solid. Taking advantage of this primary advantage of WAAM for sustainability results in a threefold reduction in energy consumption and a reduction in material waste from 90% to 40%. The major reduction in environmental impact metrics is linked to the primary energy of production for the alloy; therefore, a reduction in the material requirements significantly reduces the environmental impact of production [11].

The value for CO_2 emissions is found to be significantly dependent on the conversion factor (CES [39]) from electrical energy consumption. This conversion factor is defined by the proportion of renewable energy sources used during manufacturing. In this study, where CO_2 emission values were not obtained from previous literature [9], the CES conversion factor was calculated using the average result for global energy production based on data from the BP statistical review of world energy 2021 [40], which determined that coal accounts for 36% of global energy generation. By locating manufacture of the component in regions which have transitioned to a high proportion of renewable sources, the contribution of electrical processes such as heat treatment and WAAM deposition to the carbon footprint would be greatly reduced, making the adoption of WAAM an even more attractive proposition.

3.2. Microstructural Evolution

The microstructure of WAAM-produced Inconel 625 was analysed by optical and scanning electron microscopy in the as-deposited (AD) and solution treated (ST) conditions, with the results shown in Figures 7 and 8. These micrographs reveal a significant fraction of the detrimental Laves phase in the AD condition, while, in the ST condition, these have been entirely dissolved. A columnar dendritic structure is present in both conditions, though the distinction between dendritic and interdendritic spaces is reduced following solution treatment, suggesting homogenisation. Strengthening primary carbides (MC) are present in both conditions, while grain boundary carbides ($M_{23}C_6$) have developed following solution treatment.

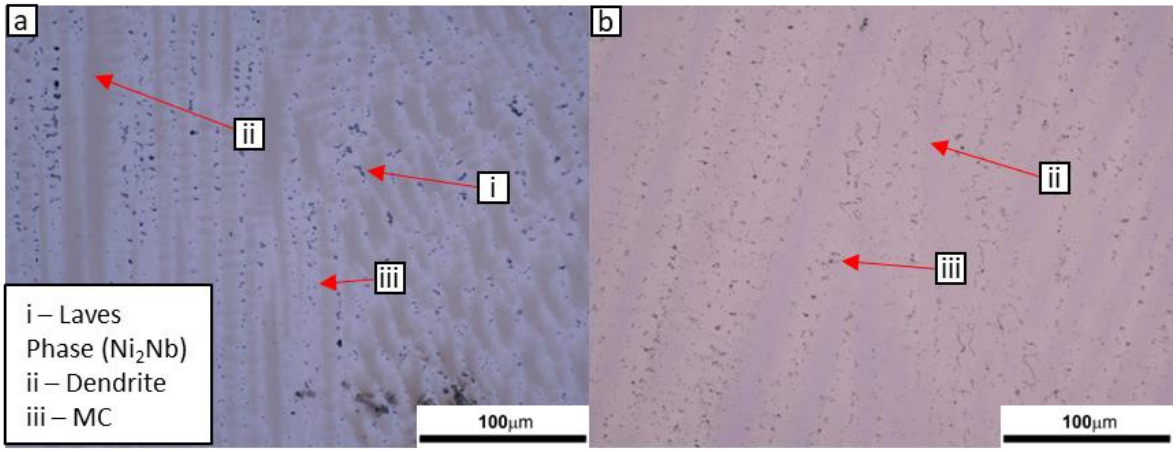

Figure 7. Optical micrographs of WAAM-deposited Inconel 625 in the (**a**) AD and (**b**) ST conditions.

A fully dense microstructure is observed, in addition to full dissolution of the detrimental Laves phase and homogenisation of the dendrites, following solution treatment. These factors suggest that mechanical performance will be high under tensile and fatigue testing, as the Laves phase is responsible for the embrittlement of the material through depletion of niobium which forms strengthening carbides [24].

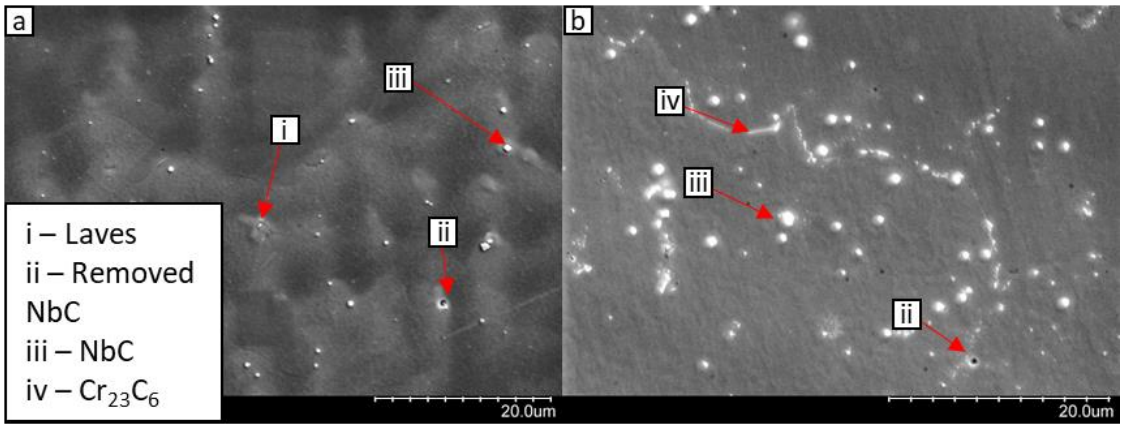

Figure 8. SEM micrographs of WAAM produced Inconel 625 in the (**a**) AD and (**b**) ST conditions.

3.3. Mechanical Property Testing

Hardness measurements were recorded on the WAAM-deposited Inconel 625 in the AD and ST conditions (Figure 9). The results present a reduction in the hardness of Inconel 625 following solution treatment. This confirms observations that the brittle Laves phase was dissolved during solution treatment, which results in the softening of the material [24,25]. In addition, the reduction in the variation of the data validates the observation that solution treatment also results in homogenisation of the material [45].

Tensile testing in the ST condition recorded a yield strength of 324 MPa, ultimate tensile strength (UTS) of 756 MPa, and elongation of 55.7%. These results are very consistent, with a standard deviation of 1.2%, 1.4% and 8.7%, respectively (Figure 10), and are compared against results from Tanvir et al. [25] and Wang et al. [46], which also detailed WAAM-produced Inconel 625. The stress vs. strain curve is presented in Figure 11. This comparison reveals that the material produced exceeds all the requirements presented in ASTM B443 [38], in addition to surpassing previously published results for UTS and elongation [25,46].

The difference between the results presented here and those from Tanvir et al. [24] and Wang et al. [46] can be explained by microstructural observations. The material presented by Tanvir et al. [24] demonstrates the presence of δ phase in the ST condition. This suggests that γ″ strengthening phases have been reduced, leading to a reduction in UTS. Wang et al. [46] tested material in the AD condition, which still contained the Laves phase, thereby leading to a reduced elongation.

Fatigue testing was performed on 15 samples at a range of maximum stresses between 100% and 160% of the yield strength of the material with the results plotted in Figure 12. These results show that the material begins to experience run-out at 100% of yield, remaining in the high cycle regime at 160% of yield; hence, it exceeds the previously published performance of wrought and welded material [28,29,47], while closely matching the results found for material produced through PM and HIP [27].

The fracture surfaces are shown in Figure 13 for both tensile and fatigue testing. On the fracture surfaces of the tensile samples, the primary failure mode observed is consistent with dimple rupture [48], with equiaxed dimples seen at the centre and elongated dimples noted at the edge of the sample. Due to the significant plastic deformation experienced by the material during tensile testing, slip planes are also observed, in addition to intergranular cracking which is expected for this material [2].

Under fatigue loading, the fracture surface is dominated by fatigue striations which are formed during the crack propagation phase. In addition, cleavage river features are identified, expanding radially from the crack initiation site. The final fracture region of the sample displays similar features to those observed following tensile testing.

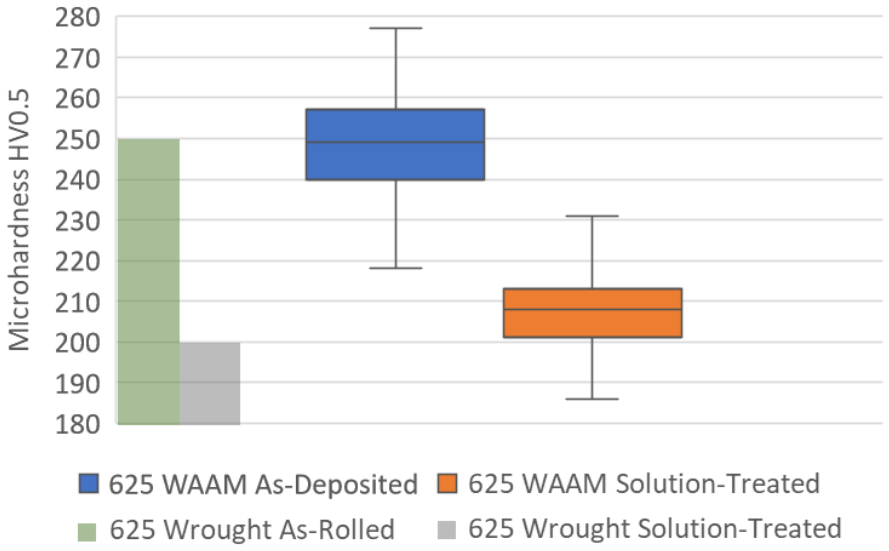

Figure 9. Microhardness values from WAAM-deposited Inconel 625 in AD and ST conditions, compared against the manufacturer's datasheet for the rolled alloy [49].

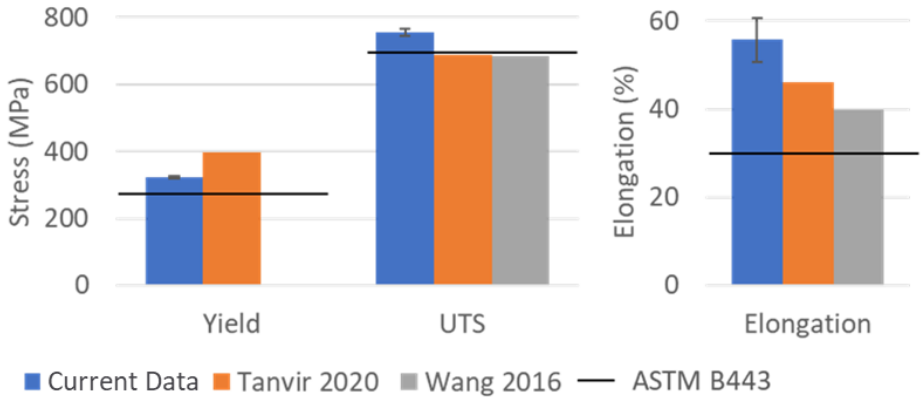

Figure 10. Results from tensile testing of WAAM-deposited Inconel 625 in AD and ST conditions compared with existing literature [24,45] and ASTM B443 [37].

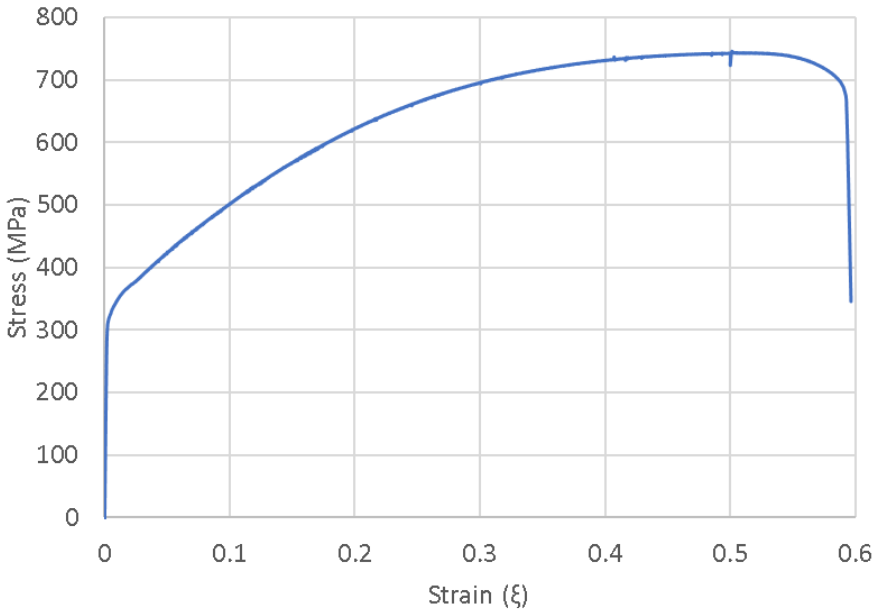

Figure 11. Stress vs. strain curve for the tensile testing of Inconel 625.

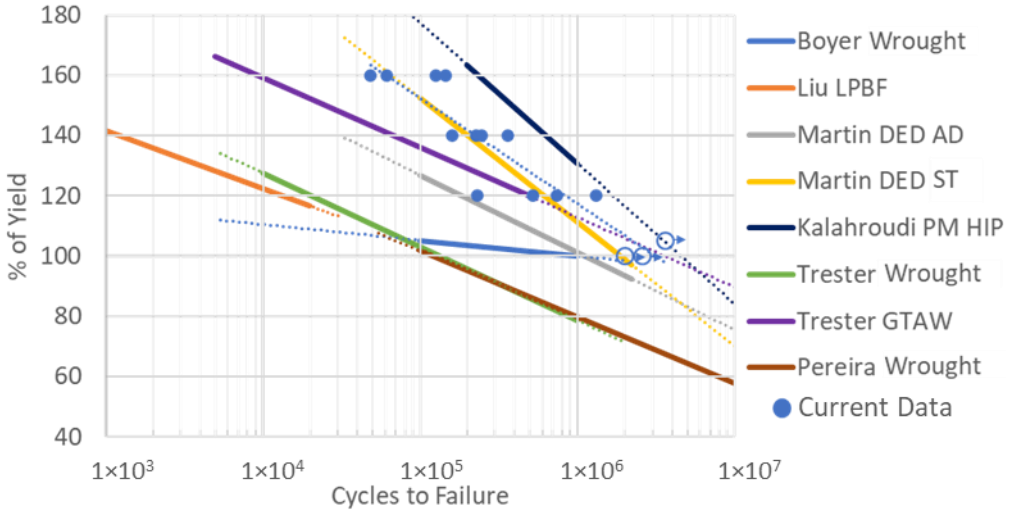

Figure 12. Results of fatigue testing for WAAM-produced Inconel 625 [26–28,39].

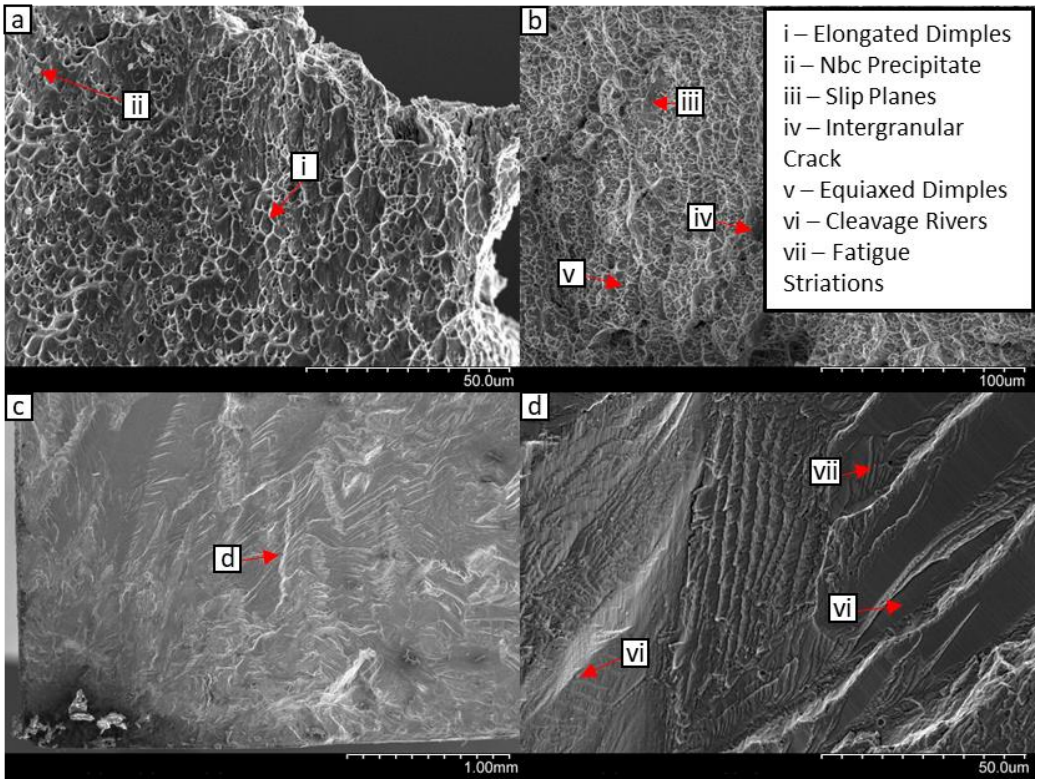

Figure 13. Fractography of tensile samples (**a**,**b**) and fatigue samples (**c**,**d**) showing representative fracture modes.

The results of tensile testing demonstrate that WAAM-produced Inconel 625 meets or exceeds the strength specified by material standards [38]. Furthermore, the strength was found to be comparable to previous studies of this combination of material and process [25,46], while the elongation was found to be superior due to a reduced development of the δ phase. This enhanced elongation was found to be beneficial to the fatigue performance of the alloy, which was superior to the wrought alloy and comparable to other AM methods [28,29,47].

The fracture surfaces were found to closely match previous results for this material, displaying dimple rupture during tensile failure, with some regions exhibiting slip planes

due to significant plastic deformation [2]. The crack propagation region of samples tested under fatigue exhibited a combination of fatigue striations and cleavage rivers.

4. Conclusions

This study has conducted an LCA on an Inconel 625 impeller and an investigation of the microstructure and mechanical properties of this alloy produced using WAAM. In both cases, the findings are compared to commercial, standard wrought materials defined by standards, previous literature and manufacturers' data sheets.

The LCA has identified a reduction in environmental impact metrics through the adoption of WAAM. A threefold reduction in energy consumption was noted, while the material waste was reduced from 85% to 35% when compared to machining. The examined microstructure was found to be free of defects, with the Laves phase being fully dissolved following solution treatment. The mechanical property testing regime demonstrated that the material meets or exceeds requirements from international standards in addition to existing literature.

When Inconel 625 components are machined from a conventional wrought alloy, their mechanical properties are satisfactory; however, the environmental impact of manufacture is high due to substantial material waste. If a WAAM process is adopted for manufacture, equivalent or superior mechanical properties are obtained, along with a dramatic reduction in the environmental impact through the reduction of waste. The CO_2 emissions can be further reduced through production in regions where renewable energy is widespread, due to the significant impact of electrical processes such as heat treatment and powering the WAAM deposition cell.

The fatigue performance of this material was also found to be enhanced compared to the wrought alloy, extending the lifespan of components. This results in a further improvement of the sustainability of using WAAM to manufacture Inconel 625 components.

Author Contributions: Conceptualization, J.I.S., A.G. and A.T.; methodology, J.I.S.; validation, J.I.S.; formal analysis, J.I.S.; investigation, J.I.S.; writing—original draft preparation, J.I.S.; writing—review and editing, J.I.S., A.G. and A.T.; visualization, J.I.S.; supervision, A.G. and A.T.; project administration, A.G. and A.T.; funding acquisition, A.G. and A.T. All authors have read and agreed to the published version of the manuscript.

Funding: This research did not receive any specific grant from funding agencies in the public, commercial, or not-for-profit sectors.

Institutional Review Board Statement: Not applicable.

Informed Consent Statement: Not applicable.

Data Availability Statement: The data presented in this study are available on request from the corresponding author. The data are not publicly available due to involvement in other unpublished work.

Acknowledgments: The authors would like to thank Glenalmond Technology for the provision of the additive manufacturing cell with which the bulk material was produced.

Conflicts of Interest: The authors declare no conflicts of interest.

References

1. Floreen, S. Metallurgy of alloy 625. In Proceedings of the International Symposium on Superalloys 718, 625, 706 and Various Derivatives, Pittsburgh, PA, USA, 26–29 June 1994; p. 13.
2. Mittra, J.; Banerjee, S.; Tewari, R.; Dey, G.K. Fracture behavior of Alloy 625 with different precipitate microstructures. *Mater. Sci. Eng. A* **2013**, *574*, 86–93. [CrossRef]
3. ASM Handbook Committee. *Properties and Selection: Nonferrous Alloys and Special-Purpose Materials*, 10th ed.; ASM International: Materials Park, OH, USA, 1990; Volume 2.
4. Huebner, J.; Kata, D.; Kusiński, J.; Rutkowski, P.; Lis, J. Microstructure of laser cladded carbide reinforced Inconel 625 alloy for turbine blade application. *Ceram. Int.* **2017**, *43*, 8677–8684. [CrossRef]
5. Wang, L.; Li, H.; Liu, Q.; Xu, L.; Lin, S.; Zheng, K. Effect of sodium chloride on the electrochemical corrosion of Inconel 625 at high temperature and pressure. *J. Alloys Compd.* **2017**, *703*, 523–529. [CrossRef]

6. Orbex. Orbex Commissions Largest Industrial 3D Printer in Europe for Rapid Rocket-Building. Available online: https://orbex.space/news/orbex-commissions-largest-industrial-3d-printer-in-europe-for-rapid-rocket-building (accessed on 3 September 2021).
7. Gradl, P.R.; Greene, S.E.; Protz, C.; Bullard, B.; Buzzell, J.; Garcia, C.; Wood, J.; Osborne, R.; Hulka, J.; Cooper, K.G. Additive Manufacturing of Liquid Rocket Engine Combustion Devices: A Summary of Process Developments and Hot-Fire Testing Results. In Proceedings of the 2018 Joint Propulsion Conference, Cincinnati, OH, USA, 9–11 July 2018; p. 2.
8. Shi, K.; Shan, D.B.; Xu, W.C.; Lu, Y. Near net shape forming process of a titanium alloy impeller. *J. Mater. Process. Technol.* **2007**, *187*, 582–585. [CrossRef]
9. *Granta Edupack 2021 R2*; Ansys-Inc.: Canonsburg, PA, USA, 2021.
10. Pang, R.; Zhang, X. Achieving environmental sustainability in manufacture: A 28-year bibliometric cartography of green manufacturing research. *J. Clean. Prod.* **2019**, *233*, 84–99. [CrossRef]
11. Sword, J.I.; Galloway, A.; Toumpis, A. An environmental impact comparison between wire + arc additive manufacture and forging for the production of a titanium component. *Sustain. Mater. Technol.* **2023**, *36*, e00600. [CrossRef]
12. *BS EN ISO/ASTM 52900:2017*; Additive Manufacturing—General Principles—Terminology. ISO: Geneva, Switzerland, 2017.
13. Benoist, V.; Arnaud, L.; Baili, M. A new method of design for additive manufacturing including machining constraints. *Int. J. Adv. Manuf. Technol.* **2020**, *111*, 25–36. [CrossRef]
14. Ngo, T.D.; Kashani, A.; Imbalzano, G.; Nguyen, K.T.Q.; Hui, D. Additive manufacturing (3D printing): A review of materials, methods, applications and challenges. *Compos. Part B Eng.* **2018**, *143*, 172–196. [CrossRef]
15. Travitzky, N.; Bonet, A.; Dermeik, B.; Fey, T.; Filbert-Demut, I.; Schlier, L.; Schlordt, T.; Greil, P. Additive Manufacturing of Ceramic-Based Materials. *Adv. Eng. Mater.* **2014**, *16*, 729–754. [CrossRef]
16. Chen, X.; Kong, F.; Fu, Y.; Zhao, X.; Li, R.; Wang, G.; Zhang, H. A review on wire-arc additive manufacturing: Typical defects, detection approaches, and multisensor data fusion-based model. *Int. J. Adv. Manuf. Technol.* **2021**, *117*, 707–727. [CrossRef]
17. Liu, J.; Xu, Y.; Ge, Y.; Hou, Z.; Chen, S. Wire and arc additive manufacturing of metal components: A review of recent research developments. *Int. J. Adv. Manuf. Technol.* **2020**, *111*, 149–198. [CrossRef]
18. Lewandowski, J.J.; Seifi, M. Metal Additive Manufacturing: A Review of Mechanical Properties. *Annu. Rev. Mater. Res.* **2016**, *46*, 151–186. [CrossRef]
19. Pan, Z.; Ding, D.; Wu, B.; Cuiuri, D.; Li, H.; Norrish, J. Arc Welding Processes for Additive Manufacturing: A Review. In Proceedings of the Transactions on Intelligent Welding Manufacturing, Singapore, 20–22 October 2018; pp. 3–24.
20. Lockett, H.; Ding, J.; Williams, S.; Martina, F. Design for Wire + Arc Additive Manufacture: Design rules and build orientation selection. *J. Eng. Des.* **2017**, *28*, 568–598. [CrossRef]
21. Evangeline, A.; Sathiya, P. Cold metal arc transfer (CMT) metal deposition of Inconel 625 superalloy on 316L austenitic stainless steel: Microstructural evaluation, corrosion and wear resistance properties. *Mater. Res. Express* **2019**, *6*, 066516. [CrossRef]
22. Silwal, B.; Walker, J.; West, D. Hot-wire GTAW cladding: Inconel 625 on 347 stainless steel. *Int. J. Adv. Manuf. Technol.* **2019**, *102*, 3839–3848. [CrossRef]
23. Wang, Y.; Chen, X.; Su, C. Microstructure and mechanical properties of Inconel 625 fabricated by wire-arc additive manufacturing. *Surf. Coat. Technol.* **2019**, *374*, 116–123. [CrossRef]
24. Tanvir, A.N.M.; Ahsan, M.R.U.; Ji, C.; Hawkins, W.; Bates, B.; Kim, D.B. Heat treatment effects on Inconel 625 components fabricated by wire + arc additive manufacturing (WAAM)—Part 1: Microstructural characterization. *Int. J. Adv. Manuf. Technol.* **2019**, *103*, 3785–3798. [CrossRef]
25. Tanvir, A.N.M.; Ahsan, M.R.U.; Seo, G.; Kim, J.-D.; Ji, C.; Bates, B.; Lee, Y.; Kim, D.B. Heat treatment effects on Inconel 625 components fabricated by wire + arc additively manufacturing (WAAM)—Part 2: Mechanical properties. *Int. J. Adv. Manuf. Technol.* **2020**, *110*, 1709–1721. [CrossRef]
26. Smith, R.A.; Hillmansen, S. A brief historical overview of the fatigue of railway axles. *Proc. Inst. Mech. Eng.* **2004**, *218*, 267–277. [CrossRef]
27. Javadzadeh Kalahroudi, F.; Sadek, M.; Krakhmalev, P.; Berglund, T.; Bergström, J.; Grehk, M. On the microstructure and high cycle fatigue of near-net shape PM-HIPed Inconel 625. *Mater. Sci. Eng. A* **2023**, *886*, 145671. [CrossRef]
28. Liu, M.; Cai, Y.; Wang, Q.; Jiang, Y.; Zou, T.; Wang, Y.; Li, Q.; Pei, Y.; Zhang, H.; Liu, Y.; et al. The low cycle fatigue property, damage mechanism, and life prediction of additively manufactured Inconel 625: Influence of temperature. *Fatigue Fract. Eng. Mater. Struct.* **2023**, *46*, 3829–3845. [CrossRef]
29. Trester, P.W.; Kaae, J.L.; Gallix, R. Fatigue strength of inconel 625 plate and weldments used in the DIII-D configuration vacuum vessel. *J. Nucl. Mater.* **1985**, *133*, 347. [CrossRef]
30. Bennett, J.; Garcia, D.; Kendrick, M.; Hartman, T.; Hyatt, G.; Ehmann, K.; You, F.; Cao, J. Repairing Automotive Dies With Directed Energy Deposition: Industrial Application and Life Cycle Analysis. *J. Manuf. Sci. Eng.* **2019**, *141*, 021019. [CrossRef]
31. Lajis, M.A.; Yusuf, N.K.; Ahmad, A. Life Cycle Assessment on the Effects of Parameter Setting in Direct Recycling Hot Press Forging of Aluminum. *Mater. Sci. Forum* **2018**, *923*, 143–148. [CrossRef]
32. Priarone, P.C.; Campatelli, G.; Montevecchi, F.; Venturini, G.; Settineri, L. A modelling framework for comparing the environmental and economic performance of WAAM-based integrated manufacturing and machining. *CIRP Ann.-Manuf. Technol.* **2019**, *68*, 37–40. [CrossRef]
33. Daniyan, I.; Mpofu, K.; Bello, K.; Muvunzi, R. Life cycle assessment for the milling operation of titanium alloy (Ti6Al4V). *Procedia CIRP* **2022**, *105*, 811–816. [CrossRef]

34. Tuan, D.D.; Wei, C. Cradle-to-gate life cycle assessment of ships: A case study of Panamax bulk carrier. *Proc. Inst. Mech. Eng.* **2019**, *233*, 670–683. [CrossRef]
35. Fricke, K.; Gierlings, S.; Ganser, P.; Seimann, M.; Bergs, T. A Cradle to Gate Approach for Life-Cycle-Assessment of Blisk Manufacturing. In Proceedings of the ASME Turbo Expo, Virtual, 7–11 June 2021.
36. Catalano, A.R.; Debernardi, L.; Balaso, R.; Rubbiani, F.; Priarone, P.C.; Settineri, L. An appraisal of the cradle-to-gate energy demand and carbon footprint of high-speed steel cutting tools. *Procedia CIRP* **2022**, *105*, 745–750. [CrossRef]
37. Bekker, A.C.M.; Verlinden, J.C. Life cycle assessment of wire + arc additive manufacturing compared to green sand casting and CNC milling in stainless steel. *J. Clean. Prod.* **2018**, *177*, 438–447. [CrossRef]
38. *ASTM-B443*; Standard Specification for Nickel-Chromium-Molybdenum-Columbium Alloy (UNS N06625) and Nickel-Chromium-Molybdenum-Silicon Alloy (UNS N06219) Plate, Sheet, and Strip. ASTM: West Conshohocken, PA, USA, 2014.
39. Jeswiet, J.; Kara, S. Carbon emissions and CES™ in manufacturing. *CIRP Ann.* **2008**, *57*, 17–20. [CrossRef]
40. BP. Statistical Review of World Energy. 2021. Available online: https://www.bp.com/content/dam/bp/business-sites/en/global/corporate/pdfs/energy-economics/statistical-review/bp-stats-review-2021-full-report.pdf (accessed on 30 January 2024).
41. *BS EN 1011-1:2009*; Recommendations for Welding of Metallic Materials. British Standard: London, UK, 2009.
42. *ASTM E8-21*; Standard Test Methods for Tension Testing of Metallic Materials. ASTM: West Conshohocken, PA, USA, 2021.
43. *BS EN ISO 148-1:2016*; Metallic Materials—Charpy Pendulum Impact Test. Part 1: Test Method. ISO: Geneva, Switzerland, 2016.
44. *E466-21*; Standard Practice for Conducting Force Controlled Constant Amplitude Axial Fatigue Tests of Metallic Materials. ASTM: West Conshohocken, PA, USA, 2021.
45. Marchese, G.; Lorusso, M.; Parizia, S.; Bassini, E.; Lee, J.-W.; Calignano, F.; Manfredi, D.; Terner, M.; Hong, H.-U.; Ugues, D.; et al. Influence of heat treatments on microstructure evolution and mechanical properties of Inconel 625 processed by laser powder bed fusion. *Mater. Sci. Eng. A* **2018**, *729*, 64–75. [CrossRef]
46. Wang, J.F.; Sun, Q.J.; Wang, H.; Liu, J.P.; Feng, J.C. Effect of location on microstructure and mechanical properties of additive layer manufactured Inconel 625 using gas tungsten arc welding. *Mater. Sci. Eng. A* **2016**, *676*, 395–405. [CrossRef]
47. Pereira, F.G.L.; Lourenço, J.M.; Nascimento, R.M.D.; Castro, N.A. Fracture Behavior and Fatigue Performance of Inconel 625. *Mater. Res.* **2018**, *21*, e20171089. [CrossRef]
48. ASM Handbook Committee. *Fractography*; American Society for Metals: Metals Park, OH, USA, 1987; Volume 12.
49. Special-Metals. Inconel 625 Datasheet; 2013. Available online: https://www.specialmetals.com/documents/technical-bulletins/inconel/inconel-alloy-625.pdf (accessed on 19 April 2024).